Application of small punch testing on the mechanical and microstructural characterizations of P91 steel at room temperature

CrossMark

M.F. Moreno [a, b, *]

[a] División Física de Metales, Centro Atómico Bariloche, Av. Bustillo 9500, 8400, S. C. de Bariloche, Argentina
[b] Consejo Nacional de Investigaciones Científicas y Técnicas, Av. Rivadavia 1917, Capital Federal, Argentina

ABSTRACT

The use of small punch test (SPT) has emerged as a potential technique for mechanical characterization using miniaturized specimens. There is a strong interest in applying SPT for life prediction of power plant components operating at high temperatures. Another important application includes implementing surveillance programs for structural materials of nuclear plants where small volumes of irradiated samples are needed. In this work the small punch test was applied to study the mechanical behavior of P91 steel at room temperature. The selection criteria of the characteristic load P_Y in terms of two methods are discussed. Using this parameter the relationship with the yield stress is studied. The correlation factors were calculated from SPT curves. Microhardness was used to detect the most strained zones in a cross section of a punched specimen when reached its maximum load. The annular zone under the ball contact area, where the plastic thinning occurred up to maximum load, coincided with the highest microhardness values. Finally, transmission electron microscopy was employed to study the final microstructures after the deformation of the tensile and small punch tested samples. Refining of subgrains and considerable increasing of dislocation density was found with both, tensile and punch tested samples. By estimation of local strain and TEM observations it was confirmed the SPT produces higher deformation than that found with tensile test after rupture.

© 2016 Elsevier Ltd. All rights reserved.

1. Introduction

The 9–12%Cr creep-resistant ferritic-martensitic steels are progressively more considered for pressure vessels, boilers, heaters and piping applications [1,2]. In particular, Grade 91 steel is widely used in the energy industry due to properties like: high creep strength, high thermal conductivity, low thermal expansion, good corrosion resistance and good mechanical properties after irradiation [3–5]. Grade 91 steel is a candidate for structural components of Generation IV nuclear power plants and future fusion reactors [1,6,7]. However, this steel could degrade its mechanical properties under thermo-mechanical cycling [8–12]. Therefore, there is an increasing demand of the accurate determination of the already mentioned properties during service. Moreover, it is also important to correlate the variation of the properties with the change of material microstructure. For this reason, miniature specimen tests are required in order to sampling without affecting the operation of

the components. Furthermore, the selectivity of the extraction of the samples becomes an advantage.

The Small Punch Test (SPT) is a technique settled for evaluating mechanical behavior from miniaturized thin disks. Typically, for this type of test, two specimen sizes are used 8–10 mm [13–15]: and 3 mm [16–18] in diameter with 0.5 mm and 0.25 mm thick, respectively. In certain cases, the disk can be obtained from a small chip extracted from a component in service without affecting its performance. For this reason, the technique could be considered as a non-destructive method. For example, SPT is very useful for creep life assessment for in-service components including welded joints [2,19,20].

The SPT can be easily described as an axis symmetrical specimen punched with a ball. The typical 'applied load vs. central disk displacement' curve for ductile steels could be divided into four different regimens [16,21]: (i) elastic bending; (ii) plastic bending; (iii) plastic membrane stretching; and, (iv) plastic instability. The geometry of the test imposes on the sample a complex stress field. The equivalent plastic strain at certain locations of the punched disk can reach values much larger than the true uniform strain [18].

* Av. Bustillo 9500, 8400, S. C. de Bariloche, Argentina.
  E-mail address: mmoreno@cab.cnea.gov.ar.

The correlations between the values determined from SPT and conventional mechanical properties are still under debate nowadays [13,15,21–24]. Most of the works on Grade 91 steels by SPT have been performed at high temperature [2,12,25–27]. To the best of the author's knowledge there are no reports over Grade 91 steel that correlate the punched specimens with their deformed microstructure after SPT analyzed by transmission electron microscopy (TEM). The combination of both techniques, SPT and TEM, in other steels has been reported only by Byun et al. [28,29] using 3 mm diameter disk. However, Fan et al. [30] reported the change of the microstructure produced by equal channel angular pressing (ECAP) over T91 at room temperature. They found that the increasing number of extrusion passes, the average grain size was gradually refined. Also, the Vickers microhardness increased in 40% for the initial sample after six ECAP passes. In the work of Zhang et al. [31], dynamic plastic deformation (DPD) is applied to modified 9Cr-1Mo steel at room temperature. They correlated the improving of tensile properties, the increasing microhardness and the changes of the microstructure processed by DPD.

The aim of this work is to associate the SPT with TEM to study the changes in microstructure of P91 steel. The deformed samples are extracted from SPT specimens to be observed by TEM. The mechanical response of P91 steel is studied using SPT at room temperature. The correlation between the flow stress and the characteristic load (P_Y) based on two different methods is discussed. Aspects regarding to the top and bottom displacement measurements are analyzed and compared.

Because of the complexity of stresses during SPT, a wide range of plastic strain is found throughout the tested specimen. The variations of such strains are distributed in both radial and thickness directions. Microhardness is used over a cross section of a tested specimen to detect the highest strained locations. The local strain is studied analyzing the microstructure by transmission electron microscopy. Finally, the microstructure of (i) a normal to the symmetry axis small punch tested sample, (ii) a radial cross section of small punch tested sample, (iii) tensile tested, (iv) as received P91 steel are compared by TEM.

2. Material and methods

2.1. Material

The material under study is the ferritic-martensitic ASTM A335 grade P91 steel provided by JFE Steel Corporation, Japan. The material was delivered in the form of pipe of 355.6 mm in diameter and 28 mm in thickness. The chemical composition is given in Table 1. The heat treatment performed by the provider was normalizing at 1050 °C for 10 min, and tempering at 785 °C for 45 min. Under these thermal treatments, the obtained microstructure of the as-received (AR) material consists in tempered martensite.

2.2. Mechanical characterizations

Cylinders with a diameter of 10 mm were obtained by machining in parallel direction to the pipe axis. A single tensile test specimen was turned from the cylinder. The thinned and polished section of the tensile test specimen had a diameter equal to 5 mm.

The tensile properties up to rupture were obtained using a servo-hydraulic MTS810 testing machine. The initial strain rate was 5×10^{-4} s^{-1}. The first part of the tensile test was monitored by an extensometer MTS 632.13F-20 with a gauge length of 10 mm.

For SPT specimens, slices of 0.9–1 mm in thickness were cut, using a diamond saw Bueler, from the same cylinder used for tensile test. Then mechanical grinding was performed to fit the thicknesses to 0.400, 0.500 and 0.600 mm with emery paper (320–2000 grit) and finally polished with 1 μm colloidal alumina suspension. In all cases the thickness variation was lower than 1%. For the small punch test it was used a special specimen holder, consisting of two dies that hold and clamp the disk-shape specimen (Fig. 1a). Fig. 1b shows the 2.5 mm diameter ball of silicon nitride in contact with the puncher and the dimensions details of the lower die. This equipment allows measuring the relative displacement between the punch and the upper die, by coupling an extensometer MTS 632.12C-20, with 25 mm gauge length.

In addition, the central displacement of the specimen was also monitored by measuring the displacement of the bottom face of the disk using a contact rode (Fig. 1a) coupled to a linear variable differential transducer (LVDT) HBM model W1T3 (±1 mm). The SPT specimens were tested at room temperature and using a constant displacement rate of 0.1 mm/min driven by an Instron 5567 testing machine. A load cell of 5 kN was used to record the applied load. In the case of sample with 0.500 mm in thickness several tests were carried out. Samples with 0.400 mm and 0.600 mm in thickness were tested only up to maximum load P_{MAX}.

Vickers microhardness testing was performed using a Mitutoyo MVK-H0 hardness tester. The load of 100 g was selected with a dwell time of 20 s. Three different conditions were evaluated: AR, broken tensile and small punched. The two directions of the AR material, i.e. transversal and longitudinal to the pipe axis, were indented a minimum of ten times. The same criterion was taken for the broken tensile specimen. The specimen in 0.500 mm in thickness was stopped at maximum load and it was carefully included, cut and polished up to 0.05 μm silica suspension. Microhardness scanning was performed on the half part of this cross section. Indentations were separated at least three indentation diagonal lengths in order to avoid local strain effect.

2.3. Microscopy observations

Different specimens were examined by optical microscopy (OM), scanning electron microscopy (SEM) and transmission electron microscopy (TEM). The bottom surfaces (opposite to ball contact face) of the SPT deformed specimens were observed by SEM FEI 515. Also, the cross section of the small punched 0.500 mm of thickness specimen was observed by OM Leica DMRM and SEM.

To study in detail the microstructural changes generated by the SPT, samples of AR, tensile and punch tested were examined by a TEM FEI CM200UT operated at 200 kV. In order to obtain a good correlation between the developed microstructure and the deformation induced by SPT, the identification of the region over which the observation is going to be performed is very important. Since the SP tested sample presents an axial symmetry, the plastic strain distribution varies both radially and across the thickness for the any load level of the stopped test. Therefore, it is essential to conduct a careful sample preparation having a spatial reference.

Table 1
Chemical composition of ASTM A335 grade P91 steel (1×10^3 wt%).

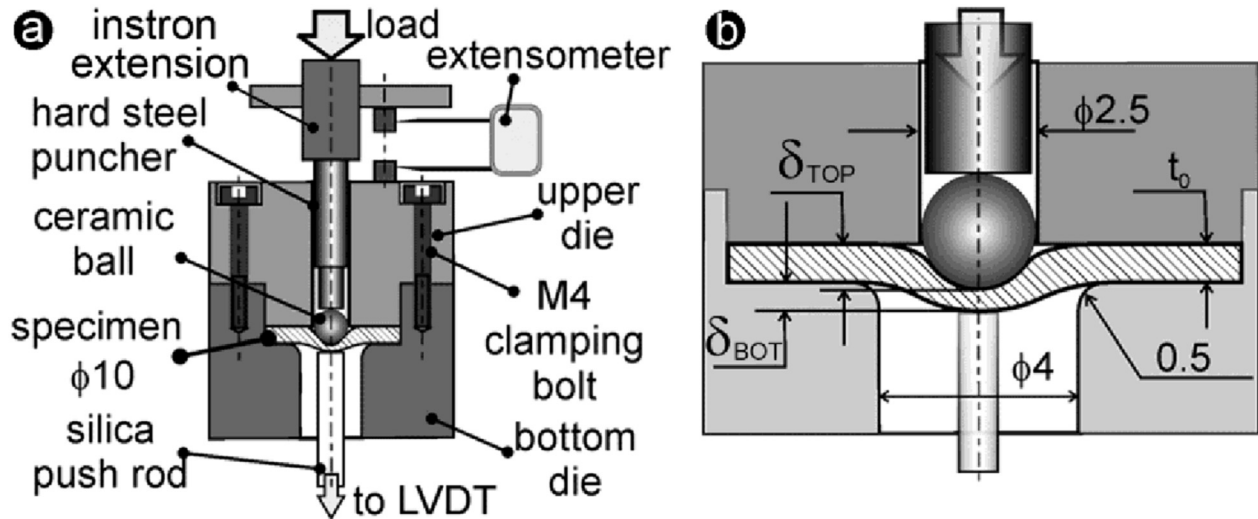| C	Cr	Mn	Si	P	S	Ni	Cu	Mo	Al	Co	Nb	Ti	V	Fe
107	9260	430	318	30	9	173	36	860	4.3	27	88	1.7	210	Bal.

Fig. 1. Schematic drawing of the small punch apparatus: (a) general view and (b) detailed view of specimen location.

In this work two different orientations of the maximum load small punch tested specimen were studied by the TEM: i) one normal to the symmetry axis and ii) radial cross section. The first kind of sample (i) was cut as a disk of 2 mm in diameter by electrical discharge machining (EDM) (see schematic picture in Fig. 2a). This cut was made keeping the ball indentation (indicated in Fig. 2b) within the TEM specimen length in order to keep a spatial reference of the test. Then, it was mechanically thinned to a thickness of (100 ± 10) μm. After thinning, sample was electropolished by a double jet TENUPOL 5, checking every 20 s that the indentation will not be erased. Optimum thinning conditions were obtained using a solution composed of 90% ethanol and 10% perchloric acid at $-1\ ^\circ$C and 15.5 V. The ultimate thinning was performed in an ion mill PIPS GATAN 691, operated at 5 keV. The region observed by TEM was at 580 μm of the symmetry axis (indicated with the white arrow in Fig. 2c) of the SPT specimen. The second kind of sample (ii), a slice of cross section of the SPT specimen was cut with a Buehler metallographic saw. The slice of 10 mm of length × 180 μm of thickness was then cut by EDM in order to reduce the length to 3 mm. This sample was carefully glued by epoxy resin in order to avoid deformation during further care mechanical grinding up to thickness of 40 ± 10 μm. Finally the sample was thinned in the ion milling, operated at 5 keV and 3.5 keV. A sequence of optical images was taken during thinning in order to follow the shape evolution to keep as a reference the ball indentation.

3. Results and discussion

3.1. Small punch testing

Fig. 3a shows the load vs. LVDT displacement for the three thicknesses: 0.400 mm, 0.500 mm and 0.600 mm. The inset in the Fig. 3a shows a detail of the beginning of the tests. Because of the difference of stiffness specimens, the initial linear plots representative of elastic behavior, show the higher slopes as the thickness increases. In order to evaluate the reproducibility of the technique several tests were repeated with the 0.500 mm specimen up to different load values, including maximum and rupture loads. Superimposing the curves of the tests a very good reproducibility along the whole test could be observed. For instance, the rupture test (continuous line data) is shown in Fig. 3a coincident with maximum load test.

The comparison of the SPT curves in Fig. 3a for the three thicknesses resulted in two main features: P_{MAX} is reached at the same displacement, and the behavior of the plots is the same. The curve can be separated in four different regimens of deformation: I-elastic bending, II-plastic bending, III membrane stretching and IV plastic instability. These regimens are defined by dotted lines for 0.500 mm sample in Fig. 3a. Same evolution was reported for three different tempering treatments of T91 at room temperature by Serre et al. [26]. The regimes limits are defined using characteristic
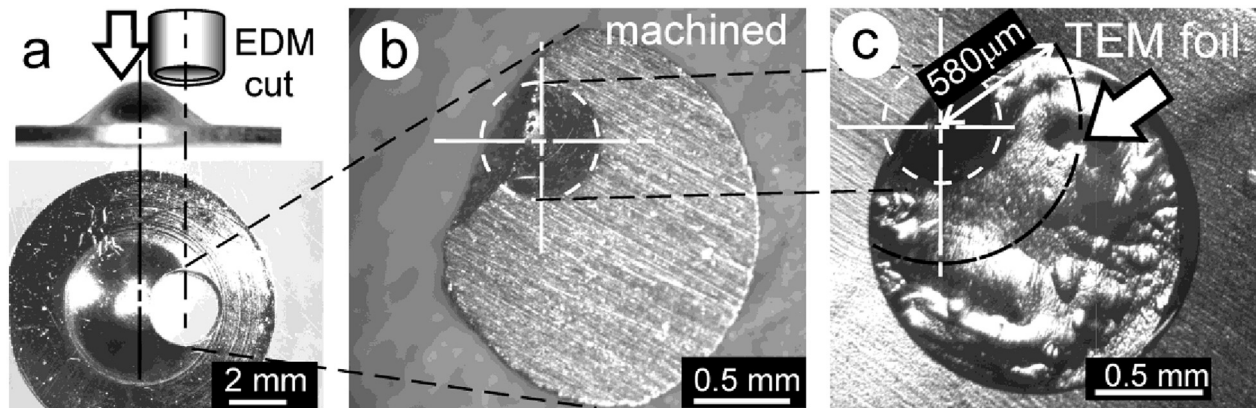

Fig. 2. Sample normal to the symmetry axis (a) EDM cut (b) after the mechanical polishing (c) final TEM foil, the ball indentation is indicated with a white dashed line.
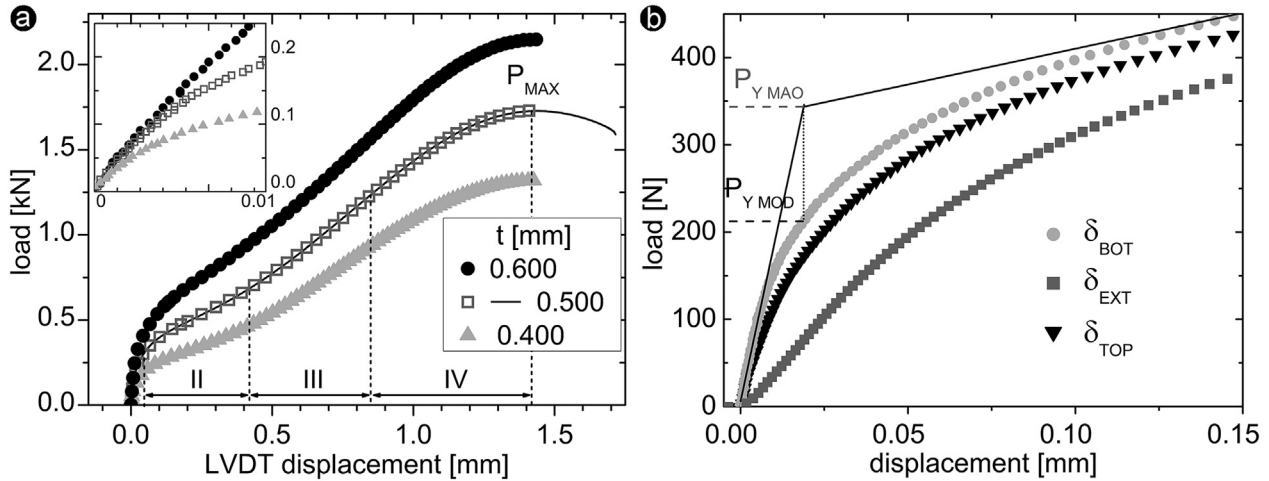
Fig. 3. (a) SPT curves of the three thicknesses, detail of initial part of tests. (b) Measured and corrected displacements during regimes I and II.

points of the curve [16,21]. The first linear region is mainly representative of elastic bending. The beginning of the second regimen is defined by a clear change in the slope of the curve. In order to define the limit between both regimens, the characteristic load (P_Y) is calculated using the SPT curve. The σ_Y is the yield stress of the material is related with P_Y by many authors using the following equation in general form [21]:

$$\sigma_{YS} = \alpha \left(P_Y / t^2 \right) + \beta \tag{1}$$

where t the initial thickness of the sample, α is a correlation factor, and β is an independent coefficient. Different methods to find P_Y were discussed in detail by García et al. [21]. These methods are still under debate, and the physical meaning of P_Y is not yet clear. To go in deeper understanding, many experimental and modeling studies [13—18,20—23,32] have been made. Other criteria [21], have shown P_Y as the load corresponding to the end of linearity in the first regime, similar to engineering criterion to calculate the offset value of $\sigma_{YS0.2}$ in tensile test.

Most of the SPT studies measured only the displacement of the puncher [17,18,21] or the displacement of crosshead testing machine [16]. In this work, the displacement of the center of the disk was recorded following two different methods. One method measures the relative displacement δ_{EXT} between the puncher and the upper die. For that purpose a coupled extensometer was used (shown in Fig. 1a). The other method measures the displacement of the bottom of the sample δ_{BOT} with a LVDT (Fig. 1a). The load as a function of the displacements curves are shown in Fig. 3b. Both methods of measurement are detailed for regimens I and II are shown in order to clear distinguish the differences. For the same load, the values of displacement are higher using the extensometer (square data) than those from the LVDT (circle data). The difference between them can be attributed to two different phenomena. First, δ_{EXT} includes the extra elastic displacement of load transmission system: Instron extension, puncher and ball. Second, the displacement of the elastic and plastic indentation is recorded by δ_{EXT}. During the regime I the plastic volume is concentrated in a reduced zone close to indentation zone [23,29]. A calibration test was performed in order to correct the extensometer displacement measurements from compliance effects. The load vs. extensometer displacement curve was performed over a tungsten carbide specimen of 1.9 mm of thickness. The unloading curve represents the

compliance of the components of the load transmission system. Then, the corrected extensometer displacement data δ_{TOP} could be computed by subtracting the compliance to the δ_{EXT} values. Corrected extensometer data represent the true displacement of the contact point between the ball and the center of the disk. The δ_{TOP} data are plotted in Fig. 3b (black triangles data). At the same load value, the δ_{BOT} is still lower than the δ_{TOP}. Thus this difference is representative of elastic and plastic ball indentation in the disk.

Other important difference between the δ_{TOP} and δ_{BOT} curves is observed in Fig. 3b. The load as function of the δ_{BOT} has a linear behavior in region I (circle data in Fig. 3b). However, δ_{TOP} measurement shows a continuous curvature (triangle data in Fig. 3b). Summarizing, there are two important points that should be highlighted regarding δ_{BOT} measurement (circle data in Fig. 3b). i-it is a direct method of measurement so, neither corrections nor calibrations should be performed in the displacement data; ii-it defines a linear behavior, representative of pure elastic response, without any effect of plastic indentation. This elastic behavior can be observed in region I in Fig. 3b up to about 100 N.

Only few works analyzed the difference between top and bottom displacements. On the one hand, Byun et al. [28,29] measured the displacement difference between the LVDT attached to the crosshead of the tensile machine and the LVDT in contact with the bottom face of the sample. They specifically showed the shifting to higher values in displacement for top data respect to bottom data in the load vs. displacement curve along the whole test. In addition, bottom data for region I was negligible in the work of Byun. On the other hand, Jitsukawa et al. [33] performed SPT with a similar configuration of both measurements. They found the same shifting of puncher displacement to higher values. However, during regime I a well-defined linear region I for bottom displacement was found. Both group of authors used a TEM-size 3 mm diameter samples with 0.25 mm of thickness. Neither of those works made corrections for the top data. The SPT is not a standardized technique yet, but an effort has been made with recommendations from the European Code of Practice [13]. This document recognizes the chance to measure both displacements (referring to the puncher displacement as "deflection"). In this reference, the deflection data can be used to analyze the SPT curve (e.g. calculus of P_Y), but no corrections to discount the compliance effects are suggested. Tol-oczko et al. [34] modeled with finite elements the ball displacement for the shear punch test (a similar device to the small punch apparatus). They found that the compliance of traditional testing

machines were too large for typical small displacement involved in punch tests. A better design of the puncher, increasing its stiffness was proposed. Until now, the direct displacement record of the ball contact point is not available due to experimental difficulties.

Mao and Takahashi [16] defined the characteristic load (P_{YMAO}) like the crossover of the linear fits of regimen I and II [16]. Moreover, these authors calculate the P_{YMAO} value using the load vs. central displacement curve taking in consideration only the movement of the crosshead of the tensile machine. In contrast, in this work, it was used the bottom displacement δ_{BOT} curve. The yield stress value for Grade 91 steel was measured during the tensile test $\sigma_{YS} = 512$ MPa. Then, the values of P_{YMAO} of each specimen were plotted as a function of $\sigma_{YS} t^2$ (Fig. 4). The correlation value obtained from the slope of the linear fitting (using Eq. (1).) is $\alpha_{MAO} = 0.37$. Here, it should be pointed out that fitting was performed assuming $\beta = 0$ (Equation (1)). This means that σ_{YS} should be equal to zero when P_Y is zero. The correlation factors found by this method for other ductile steel were between 0.32 and 0.45 [15−18,21]. However, P_{YMAO} does not belong to the SPT curve, being higher than the corresponding for the same displacement. For this reason, an alternative characteristic load called 'P_{YMOD}' is defined in this work as the vertical projection of P_{YMAO} on the load vs. δ_{BOT} curve (Fig. 3b). This methodology is similar to that found in Code of Practice cited in Ref. [13] used to define P_{Y_CEN}. The same calculations of $P_{Y\,MOD}$ are performed in the load vs. displacement curves of the samples that were 0.400 and 0.600 mm in thickness (not shown). Then the values of $P_{Y\,MOD}$ were plotted as a function of $\sigma_{YS} t^2$ (Fig. 4). The resulting correlation value was $\alpha_{MOD} = 0.55$. For both methods using P_{YMAO} and $P_{Y\,MOD}$ the linearity of the fittings was evaluated by the parameter r^2 and satisfactory results were obtained.

3.2. Microhardness and plastic strain

Fig. 5a shows the left half of the radial cross section of the 0.500 mm specimen loaded up to P_{MAX} (Fig. 3a). Indentations
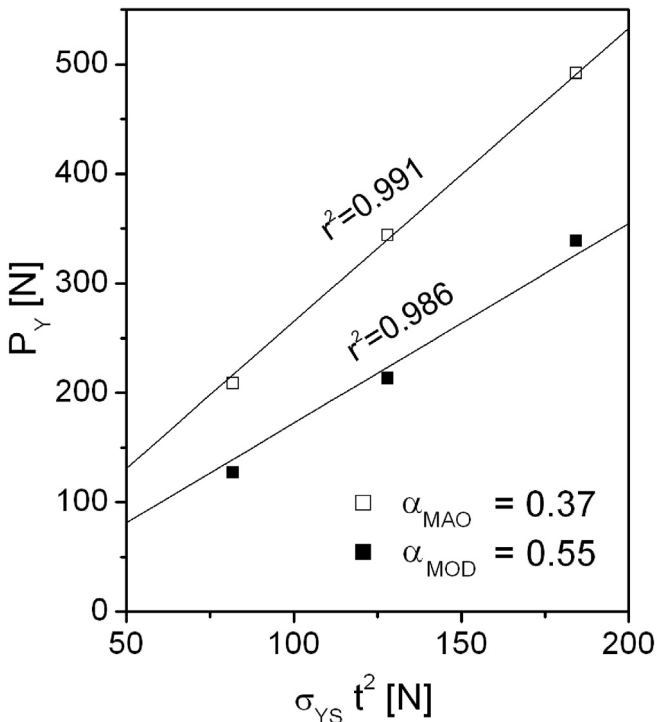
Fig. 4. Calculus of correlation factors using two different methods.
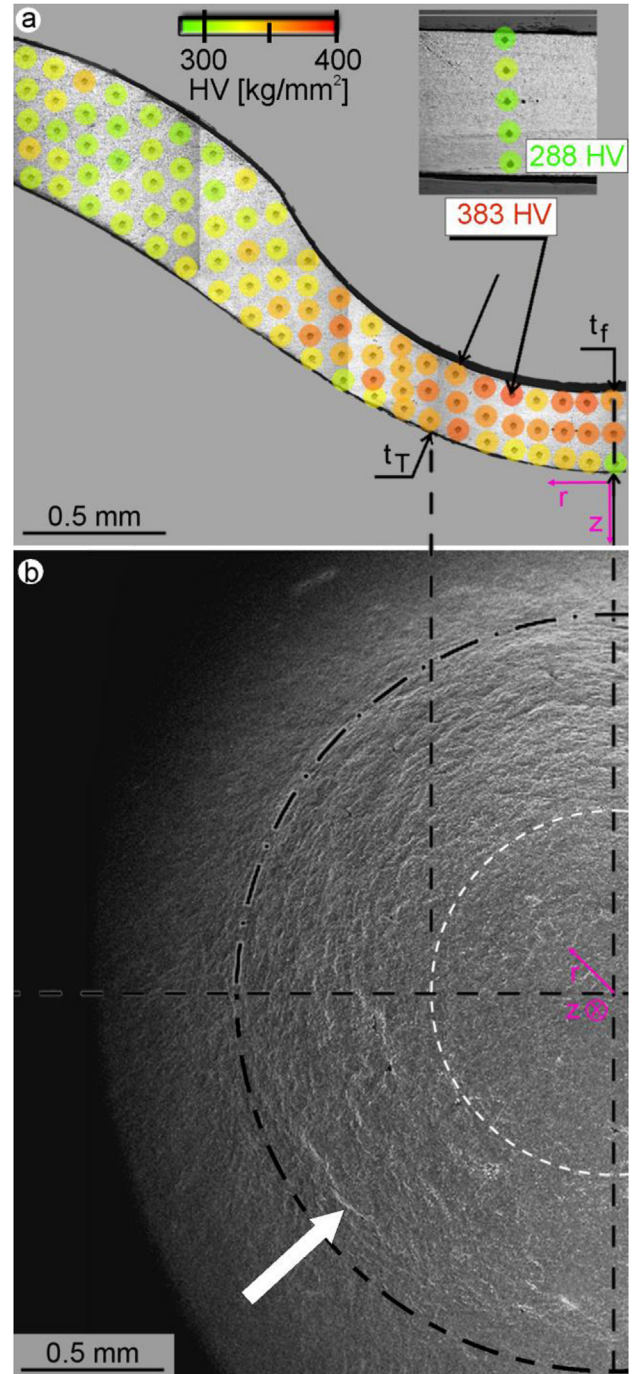
Fig. 5. (a) Optical micrograph of the left half radial cross section of the 0.500 mm of thickness specimen loaded up to P_{MAX}. (b) SEM micrograph of figure a, view from the opposite side of ball indentation.

surrounded by color scale circles are shown in this figure. Vickers microhardness (HV) values obtained are associated to the upper center colored-scale. The resulting indentations should be enough small to cover several measurements through the thinnest zone of thickness. The separation between each other indentations should be at least the length of three times the diagonal size. The load for hardness tests should be in the range where the hardness is kept constant for this material. It is known that for low loads the hardness can decrease, keep constant or increase [35]. Considering this, other load values were used as a comparison. A load of 50 g resulted

in higher HV than for 100 g, while 500 g gave similar hardness to 100 g.

The inset in the Fig. 5a shows a representative material for the non deformed region of the cross section sample (similar to AR material). The mean value of the five indentations is 288 HV $\pm$ 10. Regarding the profile shape there is a noticeable uniform thinning under the ball contact. This resulted mainly due to the plastic membrane stretching up to P_{MAX}. It can be seen that HV values vary in radial and thickness directions and the average increase of microhardness within the thinning zone is about 25%. Moreover, the punched side (upper edge in Fig. 5a) of the sample showed higher HV values than the other side of the sample. The highest value obtained is indicated with an arrow (383 HV). The increase in hardness indicates higher plastic strain due to cold deformation. The relationship between the Vickers hardness and the effective strain has been studied extensively through both experimental and analytical methods, cold upsetting and finite element modeling are examples of them [36]. For some structural steels, within the range of effective strains up to about 0.8, experimental data showed a kind of a logarithmic growth of hardness with the effective strain [36,37]. Sonmez et al. [37] proposed an analytical relation to model this Vickers hardness vs. effective strain behavior. They used the mechanical properties obtained from tensile tests from many steels with hardening behavior to validate their analytical model.

The microhardness measured after the tensile test is equal to 338 HV $\pm$ 5. This increase of about of 17% was measured out of necking volume when the strain reached about 0.2. Fan et al. [30] found an increment in the hardness of 30% after three ECAP passes without annealing after each pass. Therefore, the largest increment of the hardness obtained by SPT (383 HV) respect to AR material is similar to that obtained from some severe plastic processes. In addition, Zhang et al. [31] found a fast increase of about 60% in microhardness at high strain rates by dynamic plastic deformation (DPD). In this case the strain reached by DPD was about 1. The aim of both works, ECAP and DPD, was to enhance the mechanical properties, and the main microstructural feature characterized by TEM was reduction of subgrain size. For other plastic processes applied in ductile steels similar hardening with less pronounced increasing behavior was found [37]. Therefore, in basis of microhardness distribution of punched profile of Fig. 5a, the relative increase of plastic strain should be more pronounced than that increase detected in microhardness. Regarding analytical modeling of strain distribution on SPT, Campitelli et al. [18] modeled the deformed profile in radial cross section of TEM-size 3 mm diameter disk of 316L stainless steel. Using those FEM results, the effective strain distribution through the cross section profile for a fixed punch displacement of 0.1 mm was calculated. At that point the model showed that the highest strains were located in an annular region close to bottom side of punched specimen.

Also, two important thicknesses are indicated in the Fig. 5a: the final thickness in the center of the disk (t_f) and the lowest thickness over the cross section (t_T). The first one, t_f = 0.265 mm, is close to the original thickness 0.500 mm subtracting the difference between δ_{BOT} and δ_{TOP} after unloading the sample. As it was discussed previously, the thinning during test can be recorded from difference between the top and bottom measurement of displacement. The second thickness labeled on Fig. 5a, t_T = 0.250 mm is the smallest thickness of the deformed profile. Fig. 5b shows a left half of SEM micrograph of the bottom side of the specimen loaded up to P_{MAX}. Here, it could be appreciated an annular region with a high plastic deformation. This region is indicated between two different half circles. The first one (dash white lines) at r = 0.650 mm, the second at r ~ 1.1 mm (point dash black lines). In addition, a close similar deformation was observed on the surface of tempered T91 sample after SPT up to fracture [26]. A detailed examination of

Fig. 5b showed that there are small cracks also oriented in circumferential direction (indicated with a white arrow in Fig. 5b). The deformation pattern and cracks initiation are compatible with the reached regime when the test was interrupted. At higher magnification the open surface of a crack shows the evidence of voids coalescence (Fig. 6), typical for ductile mechanism [26]. If the load is increased after P_{MAX}, the cracks will grow until final rupture. Two magnifications of the surface of ruptured specimen (continuous line plot in Fig. 3a) are shown in SEM images of Fig. 7. The cracks that grew were larger than those found in the P_{MAX} specimen, and they followed the same radial directions. At higher magnification, it can be seen that the ductile mechanism of the crack indicated by a white arrow is similar to Fig. 6. This damage process is detected during the test as a continuous decrease of load after P_{MAX} as the displacement value increases (final regimen plotted in Fig. 3a).

Assuming a plane stress condition, the effective strain (ε_P) could be calculated at the lowest thickness of the sample (t_T) [16]. This relationship is expressed in the equation:

$$\varepsilon_P = \ln(t_0/t_T), \qquad\qquad (2)$$

where t_0 stands for the initial thickness of the sample (0.500 mm). As it was mentioned the lowest thickness is equal to 0.250 mm. For that particular thickness ε_P = 0.67. Same calculus of effective strain was made for the center disk thickness t_F obtaining ε_P = 0.63. For both locations t_T and t_f, the strain is more than three times higher than that obtained until the fracture of the uniaxial tensile test. The difference between t_f and t_T paths is the microhardness variation. There is variation of 25% through t_f between bottom (green HV value is close to AR in Fig. 4a) and the middle indentation. In contrast, according with Fig. 5a, the microhardness through t_T shows small variations. Works of [16] and [21] used the expression (2) for final thinnest ligament after fracture SPT. That is, when the plastic necking process took place. However, in this work through the analysis of the profile shape of Fig. 5a, the average effective strain was calculated when a continuous thinning is developing, and no necking is present.

Summarizing, the level of plastic deformation and microhardness were used as references to identify the most deformed regions for further extraction of TEM foils. These foils represent the final state of heavily deformed microstructure after complex stress state induced by SPT.
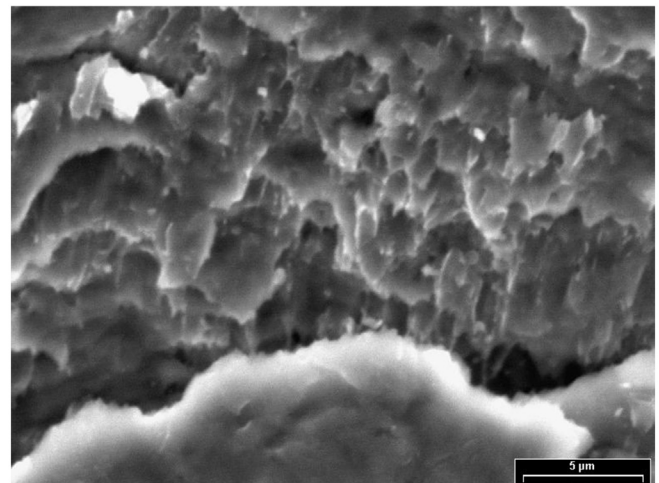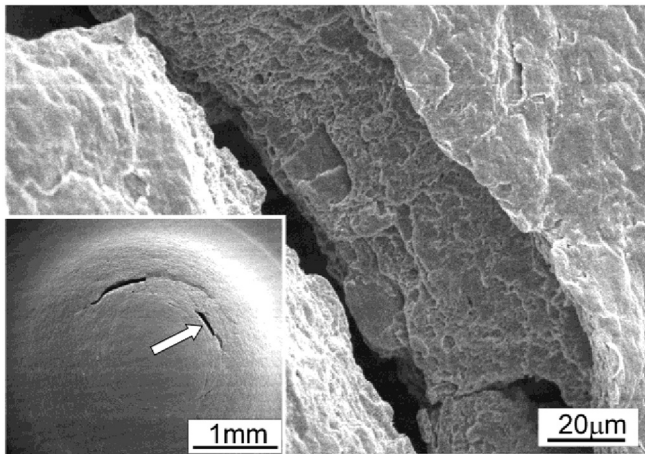

**Fig. 6.** Ductile mechanism from crack indicated in Fig. 5b.

Fig. 7. Specimen of 0.500 mm thickness after rupture punch test, general view and detail of crack surface.

3.3. TEM

The TEM analysis reveals that the microstructure of the as received material is the typical one of the 9−12% quenched and tempered steels [38]. The microstructure corresponds to tempered martensite. This microstructure has close to the body-centered cubic lattice because of the M23C6 precipitate formation during tempering. The P91 steel is composed of several microstructures at different scales, i.e. prior austenite grains, packets, blocks, laths and subgrains [38]. The as-received very fine P91 microstructure is presented in Fig. 6a. This figure shows a large amount of dislocations remaining in the material even after the tempering heat treatment. Dislocations are grouped in two sets. One set is composed of dislocations located in the subgrain boundaries. The other set is composed of dislocations located within the subgrains.

The analysis of tested samples is focused on the evolution of subgrain size and dislocation density because no differences are found at other scales. Fig. 8b shows the microstructure obtained after the tensile test. TEM analysis is done to a thin film transverse to the tensile axis. TEM film is obtained from the area out of the necking region in order to avoid the damage zone. An increment in the dislocation density is noticed by comparing Fig. 8a and b. This effect is due to an increment in the deformation of the material. The increment of dislocations is observed within the subgrains. They also form new boundaries. The formation of new subgrain boundaries produces a decrease in the average subgrain size. The dislocation density increment is in agreement with the measurements. This effect is quantified by comparing the change in the microhardness values between the as received sample and the tensile tested one. The value increases near 17%.

In the case of SPT, it is studied by TEM only the sample subjected up to P_{MAX} test. The sample subjected to test up to rupture (line plot in Fig. 3a) is not analyzed because there is a noticeable developing of surface damage (Fig. 7). So, the plastic deformation mechanisms are not the only ones occurring in the sample. Thoroughly examination of profile of P_{MAX} (Fig. 5a) test revealed only cracks on the surface, but no damage evidence inward the volume sample. The evolution of plasticity during SPT begins from indentation zone during plastic bending regime [29]. Then the plasticity extends outward, in radial direction. Finally, after plastic membrane stretching, the specimen shows an annular area with a heavy plastic deformation. A scanning along radial direction of the SPT sample is done by TEM to find the area with larger deformation features. These observations are done to correlate the deformation
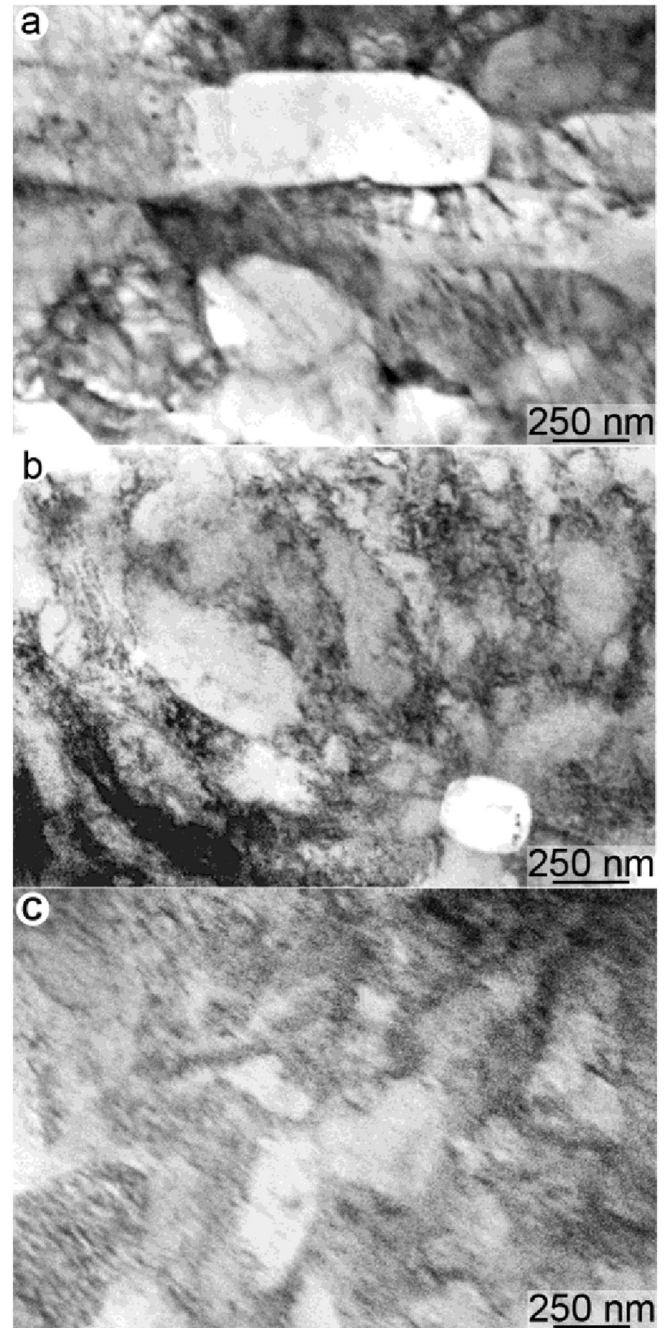
Fig. 8. Bright field images: (a) as received material, (b) tensile test sample, (c) SPT sample from puncher direction (z).

of the sample to: first, the microhardness values and, secondly, the thinnest area. It is related to the fact that microhardness tests done along to the cross section of the SPT sample characterize the most deformed area of the sample. HV values rises as the material strain increases as it was discussed in previous section. This strain increase follows a monotonic rising dependence from non-deformed material ($\varepsilon_P = 0$) up to effective strain of about 1 [37]. Fig. 8c shows the microstructure corresponding to the sample tested up to P_{MAX} observed from an axis parallel to the puncher direction. The main characteristics of the microstructure seem similar to those observed on the tensile test sample shown in Fig. 8b. Both microstructures consist of a pattern of subgrains with a complicated

dislocation structure. A detailed analysis of the micrographs of Fig. 8b and c shows that the SPT tested sample exhibits subgrains with smaller average size. It reveals the formation of new dislocation boundaries. The average dislocation density seems to increase. These observations denote an advanced deformation state in the SPT sample in comparison with the tensile test sample. In the SPT and TEM study of 316LN, Byun et al. [28] indicate that the microstructures after deformation of tensile tests and SPT are qualitatively similar. When they compare the slip line density and grain distortion are higher that those at the tensile specimen surface.

Near 580 μm from the symmetry axis (zone indicated with the white arrow in Fig. 2c), the SPT sample reveals a larger increment in the localized plastic deformation in comparison to the AR material. It must be pointed out that this thinned zone belongs to the smallest thickness detected. Because of the preparation steps, and to the reference of the ball indentation, it can be concluded that the zone of observation is located in the middle of the thickness.

Fig. 9a shows the TEM foil extracted from the cross section from P_{MAX} specimen. Two different bright field images are shown (Fig. 9b and c). Images are taken from two different areas of the cross section sample. Both micrographs are taken perpendicular to z axis defined in Fig. 5a. This direction is also represented by a cross in Fig. 9a. The area 1 is located approximately at 130 μm from the bottom surface and at 875 μm from the symmetry axis. The area 2 is located approximately at 190 μm from the bottom surface and at 920 μm from the symmetry axis. The microstructure found in area 1 is analogous to the one observed in Fig. 8b. This means that, at that point, the developed microstructure is similar to the tensile test one. According to the microhardness scanning of Fig. 5a the area 1 has almost same hardness than tensile tested specimen. An important observation can be made from the comparison between tensile and punched microstructures. While the tensile sample is representative of the material deformed under uniaxial stress, the SPT sample is subjected to more complex stresses. Although there are differences in terms of stress state, it seems that the deformation mechanisms are similar. The only difference lies in the magnification of both mechanisms; dislocation density increase and subgrains size reduction, depending on the location of the SPT sample. Thus the variation of strain in the microstructures studied by TEM is a function of the radial and thickness coordinates. This variation is in agreement with the microhardness values. Therefore, it is possible to find a wide range of strains throughout the SPT specimen, which can be representative microstructures of i-AR material, ii-rupture tensile tested or iii-a more strained microstructure. Therefore, the location of the TEM sample extraction must be carefully selected from the punched specimen.

It should be pointed out that the change in the microstructure of the SPT sample in the region of larger microhardness values is similar to the ECAP and DPD samples [30,31]. Fan et al. performed six ECAP passes over T91. With this treatment, they obtain a similar microhardness increment and they also find a similar subgrain refinement. In the work of Zhang, they produce a larger deformation of the microstructure by DPD.

Finally, the microstructure observed in Fig. 9c seems different to area 1. Area 2 reveals a larger dislocation density and subgrain boundaries start to disappear. The disappearance of them can be related to the large amount of new dislocations, which destroy the low angle boundary structures. Within the same foil in Fig. 9a, the separation between the area 1 and area 2, measured in the plane of the cross section, is about 90 μm. The different microstructures shown in Fig. 9b and c highlight two important points once again: the noticeable variation of strain in short distances, and the importance of the location to make the TEM observations.

4. Conclusions

The small punch test of ASTM 335 Grade P91 steel was performed at room temperature to evaluate its mechanical behavior up to the maximum load, for three thicknesses 0.4, 0.5 and 0.6 mm. By means of calculus of the characteristic load P_Y, the relationship to the yield stress was studied. The correlation factor was calculated using both the Mao and an alternative method. For these calculations the displacement at the bottom of the disk was used instead of the top displacement. The displacement measurement from the bottom has two important features: firstly, it is a direct method, thus no corrections are needed; and secondly a well-defined linear region representative of elastic behavior is found in this material.

The thinnest region of the cross section of the punched specimen up to its maximum load reached plastic strains more than three times the strain found up to fracture with the uniaxial tensile test. Moreover, the most deformed area of SPT specimen showed an increase of microhardness of more than 25%. The microstructural changes of both deformed specimens, tensile tested and punched were analyzed by TEM. For the small punched specimens the TEM foils were prepared in both directions, perpendicular to the symmetry axis and along the cross section. Two processes were clearly detected for tensile tested and punched specimens: the increase of dislocation density and the reduction of subgrains size. Depending on the location of the TEM observations in punched zones of the specimen, the samples showed microstructures with similar state of deformation to tensile tested or even more deformed. The magnification of the hardening processes represented by the increase of dislocation density and the reduction of subgrains size are in agreement with the increase of microhardness values. The microstructural changes induced by the SPT up to the maximum load are related to the high plastic deformation, which is similar to that found in severe plastic processes.
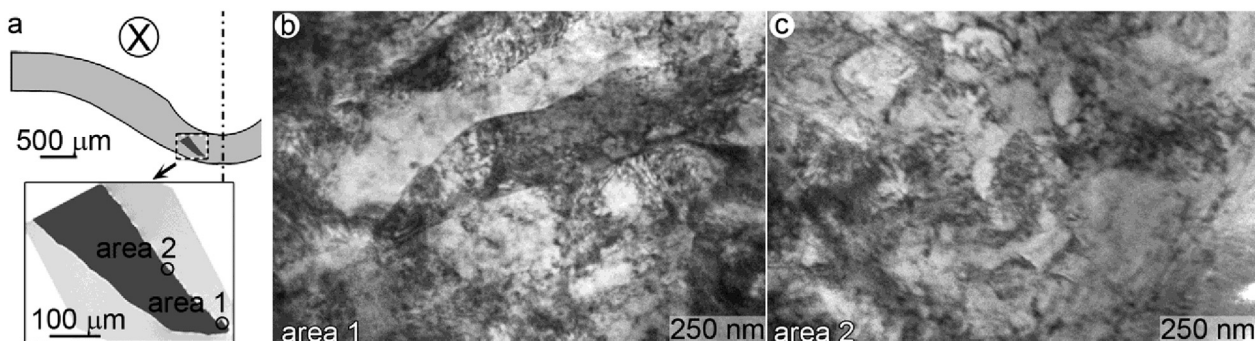

Fig. 9. (a) Scheme of the SPT cross section sample loaded up to P_{MAX} showing the position of the bright field images (b) and (c).

Acknowledgments

References

[1] Swindeman RW, Santella ML, Maziasz PJ, Roberts BW, Coleman K. Issues in replacing Cr—Mo steels and stainless steels with 9Cr—1Mo—V steel. Int. J. Press. Vessel. Pip. 2004;81(6):507—12. http://dx.doi.org/10.1016/j.ijpvp.2003.12.009.

[2] Parker J. In-service behavior of creep strength enhanced ferritic steels Grade 91 and Grade 92-part 1 parent metal. Int. J. Press. Vessel. Pip. 2013;101:30—6. http://dx.doi.org/10.1016/j.ijpvp.2012.10.001.

[3] Shamardin V, Golovanov V, Bulanova T, Povstianko A, Fedoseev, Goncharenko YA, Ostrovsky Z. Mechanical properties and microstructure of advanced ferritic- martensitic steels used under high dose neutron irradiation. J. Nucl. Mater. 1999;271—272:155—61. PII S0022-3115(98)0077.

[4] Toloczko M, Hamilton M, Malou S. High temperature tensile testing of modified 9Cr—1Mo after irradiation with high energy protons. J. Nucl. Mater. 2003;318:200—6. http://dx.doi.org/10.1016/S0022-3115(03)00023-0.

[5] Yi Y, Lee B, Kim J, Jang J. Corrosion and corrosion fatigue behaviors of 9cr steel in a supercritical water condition. Mater. Sci. Eng. A 2006;429:161—8. http://dx.doi.org/10.1016/j.msea.2006.05.035.

[6] Bloom E, Zinkle S, Wiffen F. Materials to deliver the promise of fusion power — progress and challenges. J. Nucl. Mater. 2004;329—333:12—9. http://dx.doi.org/10.1016/j.jnucmat.2004.04.141.

[7] Tavassoli A-AF, Diegele E, Lindau R, Luzginova N, Tanigawa H. Current status and recent research achievements in ferritic/martensitic steels. J. Nucl. Mater. 2014;455:269—76. http://dx.doi.org/10.1016/j.jnucmat.2014.06.017.

[8] Park J, Kim S, Lee C. Effect of W addition on the low cycle fatigue behavior of high Cr ferritic steels. Mater. Sci. Eng. A 2001;298:127—36. http://dx.doi.org/10.1016/S0921-5093(00)01291-0.

[9] Shankar V, Valsan M, Bhanu Sankara Rao K, Kannan R, Mannan SL, Pathak SD. Low cycle fatigue behavior and microstructural evolution of modified 9Cr—1Mo ferritic steel. Mater. Sci. Eng. A 2006;437:413—22. http://dx.doi.org/10.1016/j.msea.2006.07.146.

[10] Giroux PF, Dalle F, Sauzay M, Malaplate J, Fournier B, Gourgues-Lorenzon AF. Mechanical and microstructural stability of P92 steel under uniaxial tension at high temperature. Mater. Sci. Eng. A 2010;527:3984—93. http://dx.doi.org/10.1016/j.msea.2010.03.001.

[11] Fournier B, Salvi M, Dalle F, De Carlan Y, Caës C, Sauzay M, Pineau A. Lifetime prediction of 9—12%Cr martensitic steels subjected to creep—fatigue at high temperature. Int. J. Fatigue 2010;32:971—8. http://dx.doi.org/10.1016/j.ijfatigue.2009.10.017.

[12] Saad AA, Hyde TH, Sun W, Hyde CJ, Tanner DWJ. Characterization of viscoplasticity behaviour of P91 and P92 power plant steels. Int. J. Press. Vessel. Pip. 2013;111—112:246—52. http://dx.doi.org/10.1016/j.ijpvp.2013.08.001.

[13] CEN Workshop Agreement, CWA 15627:2006 E. Small punch test method for metallic materials. Brussels: CEN; 2006.

[14] Blagoeva DT, Hurst RC. Application of the CEN (European Committee for Standardization) small punch creep testing code of practice to a representative repair welded P91 pipe. Mater. Sci. Eng. A 2009;510—511:219—23.

[15] Fleury E, Ha JS. Small punch tests to estimate the mechanical properties of steels for steam power plant: I. Mechanical strength. Int. J. Press. Vessel. Pip. 1998;75:699—706.

[16] Mao X, Takahashi H. Development of a further-miniaturized specimen of 3mm diameter for TEM disk (ϕ3 mm) small punch tests. J. Nucl. Mater.

[17] Finarelli D, Carsughi F, Jung P. The small punch tests at FZJ. J. Nucl. Mater. 2008;377:65—71. http://dx.doi.org/10.1016/j.jnucmat.2008.02.053.

[18] Campitelli EN, Spätig P, Bonadé R, Hoffelner W, Victoria M. Assessment of the constitutive properties from small ball punch test: experiment and modeling. J. Nucl. Mater. 2004;335:366—78. http://dx.doi.org/10.1016/j.jnucmat.2004.07.052.

[19] Izaki T, Kobayashi T, Kusumoto J, Kanaya A. A creep life assessment method for boiler pipes using small punch creep test. Int. J. Press. Vessel. Pip. 2009;86:637—42. http://dx.doi.org/10.1016/j.ijpvp.2009.04.005.

[20] Zhao L, Jing H, Xu L, Han Y, Xiu J, Qiao Y. Evaluating of creep property of distinct zones in P92 steel welded joint by small punch creep test. Mater. Des. 2013;47:677—86. http://dx.doi.org/10.1016/j.matdes.2012.12.032.

[21] García TE, Rodríguez C, Belzunce FJ, Suárez C. Estimation of the mechanical properties of metallic materials by means of the small punch test. J. Alloy. Compd. 2014;582:708—17. http://dx.doi.org/10.1016/j.jallcom.2013.08.009.

[22] Dobeš F, Dymáček P, Besterci M. Estimation of the mechanical properties of aluminium and an aluminium composite after equal channel angular pressing by means of the small punch test. Mat. Sci. Eng. A 2015;626(25):313—21. http://dx.doi.org/10.1016/j.msea.2014.12.054.

[23] Sainte Catherine C, Messier J, Poussard C, Rosinski S, Foulds J. Small punch test: EPRI -CEA finite element simulation benchmark and inverse method for the estimation of elastic plastic behavior. In: Sololov MA, Landes JD, Lucas GE, editors. Small Specimen Test Techniques: Fourth Volume, ASTM STP 1418. West Conshohocken, PA: ASTM International; 2002.

[24] Rasche S, Kuna M. Improved small punch testing and parameter identification of ductile to brittle materials. Int. J. Press. Vessel. Pip. 2015;125:23—34.

[25] Milicka K, Dobes F. Small punch testing of P91 steel. Int. J. Press. Vessel. Pip. 2006;83:625—34. http://dx.doi.org/10.1016/j.ijpvp.2006.07.009.

[26] Serre I, Vogt J-B. Liquid embrittlement of T91 martensitic steel evidenced by small punch test. Nucl. Eng. Des. 2007;237:677—85. http://dx.doi.org/10.1016/j.nucengdes.2006.07.007.

[27] Gülçimen B, Durmus A, Ülkü S, Hurst RC, Turba K, Hähner P. Mechanical characterisation of a P91 weldment by means of small punch fracture. Int. J. Press. Vessel. Pip. 2013;105—106:28—35.

[28] Byun TS, Lee EH, Hunn JD, Farrell K, Mansur LK. Characterization of plastic deformation in a bend disk. J. Nucl. Mater. 2001;294:256—66. http://dx.doi.org/10.1016/S0022-3115(01)00484-6.

[29] Byun TS, Lee EH, Hunn JD, Farrell K, Mansur LK. In: Sokolov MA, Landes JD, Lucas GE, editors. "Small Specimen Test Techniques", ASTM STP 1418. West Conshohocken, Pa., USA: ASTM International; 2002. p. 267—82.

[30] Fan ZQ, Hao T, Zhao SX, Luo GN, Liu CS, Fang QF. The microstructure and mechanical properties of T91 steel processed by ECAP at room temperature. J. Nucl. Mater. 2013;434:417—21. http://dx.doi.org/10.1016/j.jnucmat.2012.12.009.

[31] Zhang ZB, Mishin OV, Tao NR, Pantleon W. Microstructure and annealing behavior of a modified 9Cr-1Mo steel after dynamic plastic deformation to different strains. J. Nucl. Mater. 2015;458:64—9. http://dx.doi.org/10.1016/j.jnucmat.2014.12.001.

[32] Madia M, Foletti S, Torsello G, Cammi A. On the applicability of the small punch test to the characterization of the 1CrMoV aged steel: mechanical testing and numerical analysis. Eng. Fail. Anal. 2013;34:189—203.

[33] Jitsukawa S, Kizaki M, Umino A, Shiba K, Hishinuma A. Methods and devices for small specimen testing at the Japan atomic energy research institute. In: Corwin WR, Haggag EM, Server WL, editors. Small Specimen Test Techniques Applied to Nuclear Reactor Vessel Thermal Annealing and Plant Life Extension, ASTM STP 1204. Philadelphia: American Society for Testing and Materials; 1993. p. 289—307.

[34] Toloczko MB, Kurtz RJ, Hasegawa A, Abe K. Shear punch tests performed using a new low compliance test fixture. J. Nucl. Mater. 2002;307—311:1619—23.

[35] Van der Voort GF. Results of an ASTM E-4 Round-Robin on the Precision and Bias of Measurements of Microindentation Hardness Impressions, Factors That Affect the Precision of Mechanical Tests. ASTM STP 1025. Philadelphia: ASTM; 1989. p. 3—39.

[36] Kim H, Lee S-M, Altan T. Prediction of hardness distribution in cold backward extruded cups. J. Mater. Process. Technol. 1996;59:113—21.

[37] Sonmez FO, Demir A. Analytical relations between hardness and strain for cold formed parts. J. Mater. Process. Technol. 2007;186:163—73.

[38] Kitahara H, Ueji R, Tsuji N, Minamino Y. Crystallographic features of lath martensite in low-carbon steel. Acta Mater. 2006;54:1279—88.